Feedback control of unstable cellular solidification fronts

A. J. Pons,[1,*] A. Karma,[1] S. Akamatsu,[2,†] M. Newey,[2] A. Pomerance,[2] H. Singer,[2,‡] and W. Losert[2]
[1]*Physics Department and Center for Interdisciplinary Research on Complex Systems, Northeastern University, Boston, Massachusetts 02115, USA*
[2]*Department of Physics, IPST and IREAP, University of Maryland, College Park, Maryland, USA*
(Received 15 August 2006; revised manuscript received 18 December 2006; published 8 February 2007)

We present a feedback control scheme to stabilize unstable cellular patterns during the directional solidification of a binary alloy. The scheme is based on local heating of cell tips which protrude ahead of the mean position of all tips in the array. The feasibility of this scheme is demonstrated using phase-field simulations and, experimentally, using a real-time image processing algorithm, to track cell tips, coupled with a movable laser spot array device to heat the tips locally. We demonstrate, both numerically and experimentally, that spacings well below the threshold for a period-doubling instability can be stabilized. As predicted by the numerical calculations, cellular arrays become stable with uniform spacing through the feedback control which is maintained with minimal heating.

DOI: 10.1103/PhysRevE.75.021602 PACS number(s): 81.10.Aj, 64.70.Dv, 81.30.Fb

I. INTRODUCTION

The control of cellular microstructures in directional solidification (DS) of dilute binary alloys is a subject of both industrial and fundamental interest [1,2]. DS is produced in the presence of a thermal gradient, G, which moves at velocity V_p. Cellular microstructures arise from the morphological instability of a planar front when the velocity of the thermal gradient is above some threshold, V_c, that depends on the gradient G and the alloy concentration. Once the planar front becomes unstable, it restabilizes (ideally) into a periodic array of solid fingers or "cells." A dynamic competition between solute diffusion, in the liquid, and capillary effects, at the moving solid-liquid interface, determines the typical cell size, but the local wavelength or cell spacing, Λ, admits a wide range of stable values. When the average cell spacing, Λ_0, is above some spacing threshold, Λ_c, the array is stable and achieves a steady configuration. When $\Lambda_0 < \Lambda_c$, some cells, generally those of larger local wavelength, grow faster than their neighbors. This leads to the amplification of some modes and, eventually, to the elimination of, approximately, one cell out of two [3,4] (period-doubling instability). During the initial evolution of the cell array, the elimination process is repeated, increasing progressively Λ_0, until a stable configuration with $\Lambda_0 > \Lambda_c$ is reached.

In a previous experimental work, Lee and Losert [5] (see also [6]) have shown, using the so called "combing method," that it is possible to select a uniform cell spacing within the stable range. The combing method consists of using strong local temperature perturbations in the vicinity of the front during the initial transient evolution. The thermal perturbation sets the periodicity to the cell array. However, a permanent control of cellular patterns outside the stability domain had not yet been achieved. In this paper, we propose a scheme to achieve this control and demonstrate its feasibility in both phase-field simulations and experiments. Our scheme works, essentially, by slowing down the growth of any cell which overgrows the average position of other cells in the direction of growth y. For this purpose, we apply local heating close to the protruding cell tips. A key feature of this scheme is that the amplitude of feedback perturbations (i.e., the magnitude of heating) essentially vanishes in the controlled state.

In Sec. II we present our numerical calculations. They are performed using a modified version of a recently proposed quantitative phase-field model of binary alloy solidification [7–10]. Our experimental results are shown in Sec. III. In the experiments, we used a transparent model alloy, namely, succinonitrile (SCN)-coumarin 152 (C152), in thin-sample directional solidification (see, e.g., Ref. [5] and references therein). Finally, some conclusions are stated in Sec. IV.

II. NUMERICAL RESULTS

In the numerical calculations, we use a feedback control scheme which is a simple step function, i.e., the amount of heat injected in a spotlike region is constant regardless of how far the targeted cell grows beyond the average cell position $\bar{y}$. We consider an array of N cells in a rigid box (with no-flux boundary conditions). For a given cell q, local heating at the tip is applied when the distance from the average cell position, $y_q - \bar{y}$, is larger than a predefined cutoff $\delta > 0$—a similar cutoff (about one pixel) was also introduced in our experimental feedback program (see below). The temperature field $T(\mathbf{x},t)$, neglecting the production of latent heat ("frozen temperature approximation"), can be expressed as follows:

$$T(\mathbf{x},t) = T_0 + G(y - V_p t) + p(\mathbf{x},t), \tag{1}$$

*Electronic address: a.pons-rivero@neu.edu
†Permanent address: INSP, CNRS UMR 8875, Universités Paris VI and Paris VII, 140 rue de Lourmel, 75015 Paris, France.
‡Permanent address: Laboratorium für Festkörperphysik, ETH, CH-8093, Hönggerberg, Zürich, Switzerland.

TABLE I. Parameters for impure succinonitrile used in phase-field simulations [11]. See also Ref. [10].

$\lvert m\rvert c_\infty$ (shift in melting temperature)	2 K
D (diffusion coefficient)	10^{-9} m^2/s
Γ (Gibbs-Thompson coefficient)	6.48×10^{-8} K m
V_p (pulling speed)	32 μm/s
G (thermal gradient)	143.587 K/cm
d_0 (capillary length)	1.3×10^{-2} μm
k (partition coefficient)	0.3
ϵ_4 (0.7% anisotropy)	0.007

$$p(\mathbf{x},t)=\sum_q g\Lambda_0 H[y_q(t)-\bar{y}(t)-\delta]\exp\left(\frac{-[\mathbf{x}-\mathbf{x}_q(t)]^2}{\xi^2}\right), \tag{2}$$

where $\mathbf{x}$ is the two-dimensional vector position, $p(\mathbf{x},t)$ is the imposed thermal perturbation, $H[\cdots]$ is the Heaviside step function, and the sum extends to the N cells. These equations enter as a modification of Eqs. (132) and (133) in Ref. [10]. They approximate the fact that each heating spot in the experiments results in the build up of a Gaussian bump in the thermal field of constant width, ξ, and amplitude, $g\Lambda_0$. A precise determination of the phase diagram for the SCN-C152 alloy used in this study is presently lacking. Therefore, for sake of realism, we carry out the phase-field simulations for physical parameters (Table I) estimated in Ref. [11] for a SCN-X alloy (where X stems for an unknown impurity).

The feasibility of our control scheme is best illustrated by comparing the dynamic evolution of a strongly unstable cellular array with and without control. The wavelength of the array $\Lambda_0=11.3$ μm is well below the stability threshold $\Lambda_c\approx50$ μm for cell elimination [12]. Without control, the known spatial period-doubling instability that leads to cell elimination is observed. In contrast, with control on, this instability is suppressed. In Fig. 1, we show the evolution in time of the front position, y_q, at specific x positions that initially correspond to cell tips, when control is on. It is observed that $\bar{y}$ decreases at the same time that y_q dispersion decreases. Later, when y_q dispersion is reduced, the average position advances arriving to a steady state value. In Fig. 2 we show some snapshots of the front evolution. Due to the large initial value of $|y_q-\bar{y}|$ along the pattern, a relatively strong (or frequent) heating is necessary for melting protruding cells backwards (decreasing $\bar{y}$). This entails a transitory disorder visible in Fig. 2(b). However, this large-perturbation stage ceases as soon as cell tips reach an almost equal undercooling [Fig. 2(c)]. Eventually, a uniform pattern is stabilized [Fig. 2(d)]. In Fig. 3 we show the evolution in time of the total energy input E for one of the cells ($q=2$). E is defined as the integral in time of the Heaviside step function that appears in Eq. (2). Similar curves are obtained for the other cells (except for the less advanced one which is never heated). Two different linear regimes may be identified in these curves. Initially, E grows quickly because of the continuous heating of the protruding cells. At longer times, the slope of this curve $f=dE/dt$, which is the frequency at which the cell is being perturbed, is reduced to a much smaller value (which varies only slightly from one cell to the other). This corresponds, in our control scheme, to the minimal heating needed to maintain the controlled state. The crossover between the two linear regimes is relatively short: active control is rapidly achieved. These two important

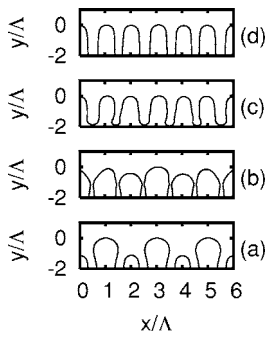

FIG. 2. Snapshots of the front evolution for the phase-field simulations shown in Fig. 1. The near cell-tip region is displayed for simplicity. Times (increasing upwards): (a) 0.0 s, (b) 0.6952 s, (c) 1.3992 s, and (d) 2.1032 s.

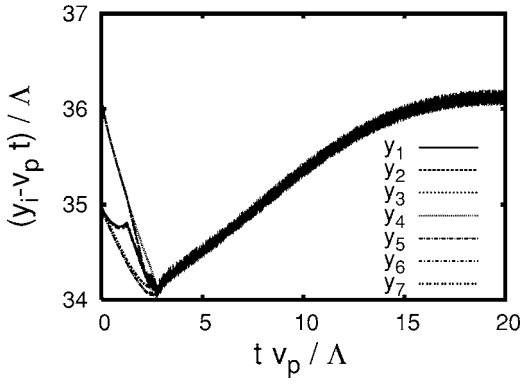

FIG. 1. Evolution in time of the tip positions, $y_q(t)$, in the growth direction referred to a given isotherm when control is on, obtained from phase-field simulations. $g/G=2.5$, $\delta/\Lambda=0.5\%$, and $\xi/\Lambda=0.97$. $\Lambda=11.3$ μm.

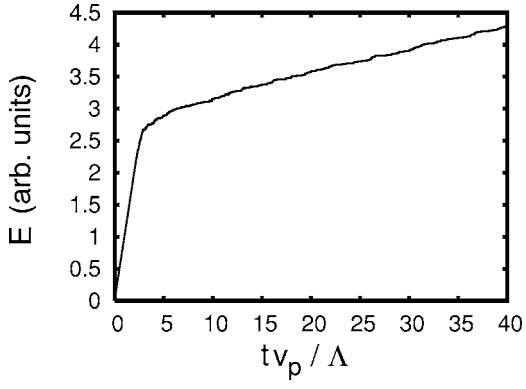

FIG. 3. Energy input, E (arbitrary units), as a function of time, t, for one of the cells ($q=2$) from the phase-field simulations shown in Fig. 1. $E(t)$ is obtained by integrating in time the Heaviside step function which appears in Eq. (2).

features—stabilization of a uniform $\Lambda(x)$ distribution and small heating frequency at long time—are also observed experimentally (see further comments in the next section).

Note also that the system could not be controlled by setting the cutoff δ equal to 0 ($\delta/\Lambda=0.5\%$ in Fig. 2). The reason for this is that it is practically impossible to maintain all tips at exactly the average fixed position. Therefore, our feedback algorithm with $\delta=0$ heats continuously some of the tips and leads to a completely melt out of cells, destroying the periodicity of the array. Naturally, feedback control also fails for large δ values (e.g., $\delta \geqslant 0.1\Lambda$).

III. EXPERIMENTAL RESULTS

In the experiments, we solidified a binary SCN-0.1 wt. % C152 alloy in a gradient $G=10\ \mathrm{K\ cm^{-1}}$, and with $V_p=2-20\ \mu\mathrm{m\ s^{-1}}$ (same device as in Ref. [5]). The alloy, which crystallizes in a bcc cubic crystal, is confined in a 100 μm thick, 2 mm wide, 150 mm long, glass-wall microtube. Prior to DS experiments, a single crystal with its [100] axis almost parallel, within less than 2°, to the solidification axis was selected by an empirical procedure and grown in such a way that it fills the container; it served as a permanent seed for further experiments. Experiments justify the use of a 0.7% anisotropy for the surface tension in the numerical calculations (see Table I) [13]. The local-heating system is a holographic laser tweezer (BioRyx200 from Arryx Inc) which consists of a 2-W NdYAG ($\lambda=532$ nm) laser that is focused onto a spatial light modulator. The single laser spot is then split into a multiple diffraction spot pattern, which is projected into the imaged region through a $(4\times)$ objective of an inverted microscope. The system software allows independent positioning of hundreds of spots into controlled arrangements. Heating in the liquid is due to partial absorption of light by the fluorescent dye [14]. In a first approximation, a laser spot (about 10 μm in diameter) acts as a pointlike source of heat which diffuses rapidly in a quasibulk medium, including the thick glass walls. A Gaussian bump superimposed to the linear gradient [see Eq. (2)] is, thus, a realistic representation of the modified thermal field. For efficient control of cellular structures, we generally tuned the (nominal) lighting power of each individual laser spot to 0.08–0.10 W. The duration of an elementary laser spot shot in our feedback control loop was of about 1.4 s in average. From a rough calibration, we estimate that for a short exposure time (of order 1 s) and 0.1 W laser power, the material is heated by less than 0.1 K in a region which extends over less than 40 μm (in the numerical simulations, the heating power corresponds to $g\Lambda_0 \approx 0.4$ K and it extends over $\xi \approx 10\ \mu$m). There is no measurable overlapping between two neighboring laser spots, which are much smaller than Λ_0 (typically 100 μm).

We image the solidification front with a (1024×1280 pixel^2) digital camera. After some image processing, the front line is detected and smoothed with a moving central average of 5 pixels and the list of tips is detected. They are subsequently sent to the laser controller after calculating the deviation from the average tip position. We use a feedback control program based on the numerical simulations to automatically place laser spots in the liquid region ahead of the protruding tips. By restricting the number of controlled spots to eight ($N=8$), we are able to update the laser spots at approximately 0.7 Hz in average.

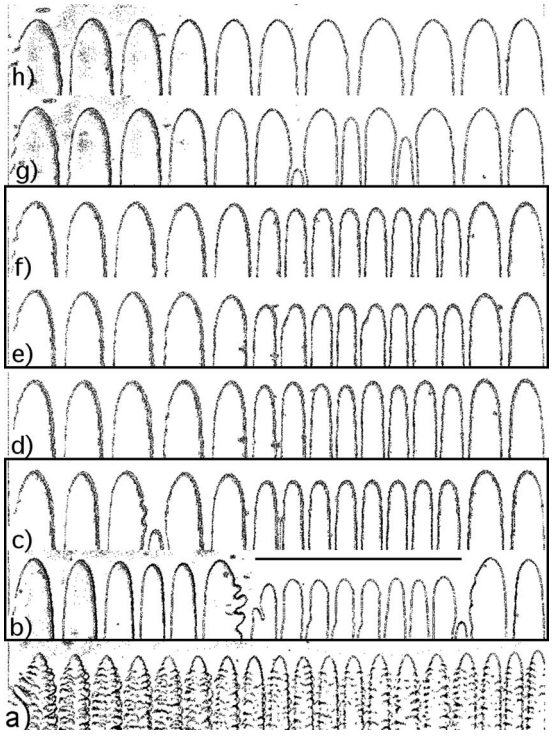

FIG. 4. Experimental sequence of images during feedback control of a small-spacing cell front pattern (time increases upwards). Also see Fig. 5. Horizontal bar: controlled region. Frames: feedback control is on. (a) Initial, high-velocity cell pattern ($t=0$; $V_p=18.4\ \mu\mathrm{m\ s^{-1}}$) obtained with the combing method (see text); (b) transient, distorted, pattern due to strong perturbations just after control is turned on ($t=1100$ s; $V_p=6.1\ \mu\mathrm{m\ s^{-1}}$); (c) stabilized pattern ($t=1520$ s; $V_p=4.6\ \mu\mathrm{m\ s^{-1}}$); (d) period-doubling instability after control has been turned off ($t=1610$ s); (e) distorted pattern after control is turned on again ($t=1620$ s); (f) restabilized pattern ($t=2100$ s); (g) highly unstable pattern (control off) ($t=2300$ s); (h) large-spacing (uncontrolled) pattern. Horizontal dimension: 2000 μm.

A sequence of images during a typical feedback control experiment is shown in Fig. 4. A simplified spatiotemporal diagram of the experiment is shown in Fig. 5. In the experiment, after a fast partial melting of the sample and formation of a planar solid-liquid interface at rest (not shown), we started pulling at relatively high velocity ($V_1 \approx 18\ \mu\mathrm{m\ s^{-1}}$). This allowed us to obtain a cellular array with small spacing by using the combing method [Fig. 4(a)]. Then, we switched off the combing laser array, turned on control, and decreased the velocity stepwise down to a final value $V_4=4.6\ \mu\mathrm{m\ s^{-1}}$ ($\approx V_1/4$) at which the pattern is unstable. After a relatively short transient, during which the pattern is strongly perturbed due to frequent illumination [Fig. 4(b)], a well controlled, small-spacing pattern is eventually obtained [Fig. 4(c)]. Note that the area accessible to the laser spot array is limited to about 1 mm, thus, only one-half of the cellular pattern may be controlled. The other half was imaged but grew freely

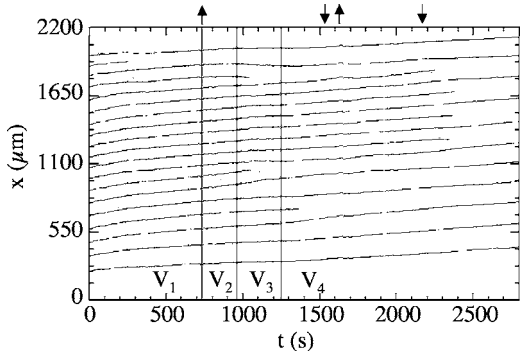

FIG. 5. Lateral cell tip position x as a function of time (same run as Fig. 4). Vertical bars: velocity jumps (V_1=18.4 μm s^{-1}; V_2=9.2 μm s^{-1}; V_3=6.1 μm s^{-1}; V_4=4.6 μm s^{-1}). Upward (downward) arrows: feedback control on (off). Lateral drift of the pattern is due to a slight misalignment of the [100] axis of the single crystal with axis y.

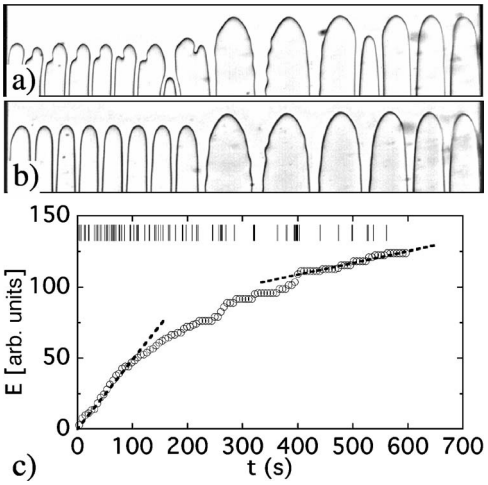

FIG. 6. Experimental control of a small-spacing cell pattern (V_p=2.9 μm s^{-1}). (a) Initial pattern (t=0). (b) Final pattern (t=580 s). The sample width (2 mm) fits into the lateral dimension of the micrographs. (c) Energy input E (arbitrary units) as a function of time t (circles) for the fifth cell from the left. $E(t)$ is obtained by summing the number of laser spot shots (vertical bars). Dashed lines: linear fits obtained at the beginning (t=0–100.8 s) and at the end (t=396.2–600.6 s) of $E(t)$ data.

without control. As it can be seen in the spatio-temporal diagram of Fig. 5, many cells are eliminated outside the controlled window, while the number of controlled cells remains constant.

After about 10 minutes of successful control, we intentionally switched the laser light off during a few minutes, and observed the onset of the period-doubling instability [Fig. 4(d)]. By turning feedback control on again, we were able to prevent cell elimination and to restabilize a small-spacing cell pattern similar to the initial one [Fig. 4(f)]. We stress the striking resemblance between numerical (Fig. 2) and experimental [Figs. 4(d)–4(f)] runs—including the transient stage after the laser is turned on [Fig. 2(b) and Fig. 4(e)]. Finally, we switched feedback control off again and let the instability fully develop, and, as expected, approximately one cell out of two is eliminated in the previously controlled area [Figs. 4(g) and 4(h)].

In Fig. 6, we show another feedback control experiment obtained following the same protocol as detailed above. In this case, the velocity was decreased to V_p=2.9 μm s^{-1}. This value is farther below the period-doubling instability threshold than the value used in Fig. 4. Nevertheless, the stabilized final spacing is nearly identical in both experiments. During the experiment shown in Fig. 6, we performed two successful feedback control runs separated by a short interruption used to check the growth rate of the instability. Time t=0 in Fig. 6 corresponds to the beginning of the second control run. At this time, the small-cell pattern is strongly disordered [Fig. 6(a)], as we have seen in Figs. 2(b), 4(b), or 4(e). We carried out feedback control during about 11 min [Fig. 6(b)]. We reproduced such feedback control experiments several times with full success for final velocities falling between 2.9 and 4.6 μm s^{-1}. The stabilized cell spacing (90–105 μm) did not vary much from one solidification run to another.

Let us make two important remarks. In numerical as well as in experimental runs, the spacing distribution in a well controlled pattern is remarkably uniform (it is not so outside the controlled area) as seen, for example, in Fig. 4(b). In addition, the controlled small-spacing cells sit slightly behind, thus have a larger undercooling than the large uncontrolled ones, as expected. This is not due to the added heat from the feedback control, but due to interactions between cells.

The second remark concerns the marked decrease of the heating power applied to the cell pattern for long-term stabilization. In our feedback control scheme, this power is given by the number, f, of laser spot exposure events ahead of cells per unit time. This f is the direct experimental analog of the slope of the energy-time curve from phase-field simulations shown in Fig. 3. We have seen that for the phase-field simulations this quantity decreases from the initial high value to smaller values when the system has been totally controlled. The same observation—f gradually decreases as control goes on, reaching a constant value for long times—has been observed for the experiments (see Fig. 6). In the graph shown in Fig. 6(c), each vertical-bar mark along the time axis corresponds to one laser spot shot ahead of the fifth cell from the left in the micrographs. The time interval between individual shots clearly increased as time was running. We also represented the integrated version of these data, E (arbitrary units). One can adjust a linear law separately at the beginning and at the end of the experimental $E(t)$ curve. We obtained $f \approx 0.5$ s^{-1} at the beginning of the run, and $f \approx 0.05$ s^{-1} 10 minutes later. These values would correspond to the two different slopes observed in Fig. 3. Let us add that the final characteristic time $1/f \approx 20$ s in our experiment is smaller than the characteristic amplification time of the period-doubling instability ($\tau \approx 80$ s) measured *in situ* in the uncontrolled, unstable pattern (not shown), observed after feedback control has been turned off definitively. Furthermore, we always performed feedback control sequences much longer (more than 10 minutes) than τ. It is interesting to note, also, that the final $1/f$ is comparable to the so-called diffusion time $\tau_d = D/V^2 = 10-100$ s (D falls in the

$10^{-10}-10^{-9}$ m^2 s^{-1} range), which signals a quasisteady regime. Therefore, control can be maintained as long as wanted.

IV. CONCLUSION

We have shown experimentally and numerically that highly unstable cellular solidification arrays can be stabilized using feedback control. Experiments and simulations showed similar dynamical evolution as the array was controlled. Unlike feedback stabilization schemes for planar fronts slightly above V_c proposed by Savina *et al.* [15], our approach stabilizes efficiently highly unstable states and can be implemented experimentally with only a discrete number of controllable heating points. An alternate control scheme which includes a tunable heating power for each spot has been implemented numerically [16]; an experimental realization is currently in progress. Although a quantitative comparison between numerical and experimental results is not yet possible because of the lack of detailed knowledge of the alloy phase diagram, the observed qualitative behaviors are identical.

The use of other localized physical perturbations generated, e.g., by x-rays or ultrasound could potentially make it possible to extend this control scheme to metallic alloys where the growth of much finer array structures with superior mechanical properties is of considerable practical interest. In addition, the ability to access experimentally unstable steady-state patterns provides an important new tool to enrich our fundamental understanding of pattern formation in directional solidification.

ACKNOWLEDGMENTS

The authors thank B. Echebarria for helpful discussions. This research was supported by NASA Grant No. NNM04AA15G, by Ministerio de Educación y Ciencia under Grant No. EX2005-0085, and by a Research Corporation Research Innovation program.

[1] W. Kurz and D. J. Fisher, *Fundamentals of Solidification*, 4th ed. (Enfield Publishing and Distribution Company, Enfield, NH, 2001).
[2] W. J. Boettinger, S. R. Coriell, A. L. Greer, A. Karma, W. Kurz, M. Rappaz, and R. Trivedi, Acta Mater. **48**, 43 (2000).
[3] J. A. Warren and J. S. Langer, Phys. Rev. E **47**, 2702 (1993).
[4] P. Kopczynski, W.-J. Rappel, and A. Karma, Phys. Rev. Lett. **77**, 3387 (1996).
[5] K. Lee and W. Losert, J. Cryst. Growth **269**, 592 (2004).
[6] W. Losert, B. Q. Shi, and H. Z. Cummins, Proc. Natl. Acad. Sci. U.S.A. **95**, 431 (1998); **95**, 439 (1998).
[7] A. Karma and W.-J. Rappel, Phys. Rev. E **53**, R3017 (1996).
[8] A. Karma and W.-J. Rappel, Phys. Rev. E **57**, 4323 (1998).
[9] A. Karma, Phys. Rev. Lett. **87**, 115701 (2001).
[10] B. Echebarria, R. Folch, A. Karma, and M. Plapp, Phys. Rev. E **70**, 061604 (2004).
[11] M. Georgelin and A. Pocheau, Phys. Rev. E **57**, 3189 (1998); Eur. Phys. J. B **4**, 169 (1998).
[12] B. Echebarria and A. Karma (unpublished).
[13] M. Muschol, D. Liu, and H. Z. Cummins, Phys. Rev. A **46**, 1038 (1992).
[14] L. M. Williams, M. Muschol, X. Qian, W. Losert, and H. Z. Cummins, Phys. Rev. E **48**, 489 (1993); **48**, 4862 (1993).
[15] T. V. Savina, A. A. Nepomnyashchy, S. Brandon, A. A. Golovin, and D. R. Lewin, J. Cryst. Growth **237-239**, 178 (2002).
[16] A. J. Pons and A. Karma (unpublished).